RSC Advances

PAPER

Cite this: *RSC Adv.*, 2021, **11**, 38578

A hybrid design of Ag-decorated ZnO on layered nanomaterials (MgAC) with photocatalytic and antibacterial dual-functional abilities†

Tuyet Nhung Pham,*[a] Nguyen Thi Hue,[a] Young-Chul Lee,[b] Tran Quang Huy,[a] Nguyen Thi Thu Thuy,[a] Hoang Van Tuan,[a] Nguyen Tien Khi,[ac] Vu Ngoc Phan,[ac] Tran Dang Thanh,[e] Vu Dinh Lam[e] and Anh-Tuan Le*[ad]

In this work, Ag@ZnO and Ag@ZnO/MgAC photocatalysts were synthesized using a simple two-step electrochemical method by the addition of magnesium aminoclay (MgAC) as a great stabilizer and a Lewis base, which could donate electrons for reduction of Ag^{+} and Zn^{2+} ions, facilitating uniform formation as well as effective inhibition of aggregation of Ag@ZnO nanoparticles (NPs) on the MgAC matrix. Ag@ZnO and Ag@ZnO/MgAC were investigated for photocatalytic degradation of MB and their antibacterial efficiencies. Ag@ZnO/MgAC showed excellent photocatalytic MB degradation with a performance of 98.56% after 80 min of visible-light irradiation and good antibacterial activity against *Salmonella* (*Sal*) and *Staphylococcus aureus* (*S. aureus*) bacterial strains, providing promising high application potential. Herein, different from the bare ZnO NPs, for Ag@ZnO/MgAC nanocomposites, Ag@ZnO NPs functioned as an effective photocatalyst under visible light illumination, in which, incorporated Ag atoms in the ZnO crystal structure caused the increase in a larger number of lattice defect sites. Benefiting from the strong surface plasmon resonance (SPR) effect of Ag and energy band matching between ZnO and Ag, the visible light absorption capacity and the separation of the photogenerated charge carriers were promoted. Therefore, the MB degradation efficiency of Ag@ZnO/MgAC was considerably accelerated in the presence of produced radicals from visible light illumination.

Received 15th November 2021
Accepted 18th November 2021

DOI: 10.1039/d1ra08365a

rsc.li/rsc-advances

1. Introduction

Zinc oxide (ZnO) is known as a typical semiconductor photocatalyst under UV light illumination with a direct bandgap (3.37 eV) in environmental pollutant treatment and a promising candidate for antibacterial applications owing to its low cost, abundant availability, non-toxicity, and great antimicrobial activity.[1–3] Unfortunately, its practical applications have still been limited because of inevitable shortcomings originating from wide bandgap, low photocatalytic efficiency, high photocorrosion and photodissolution, intrinsic structural instability, poor reusability, and ease of aggregation.[4,5] To overcome such limitations, some efforts have been recorded in assembling nanosized structures, enhancing the crystalline quality *via* the control of morphology, size, and impurity, modifying ZnO nanomaterials with noble metals, non-metals, and metal oxides, even combining carbonaceous materials and porous structural materials.[3,4,6,7] Among them, Ag, a noble metal possessing many merits in strong biocidal activity, non-cytotoxicity toward human cells, high electrical and thermal conductivity,[8,9] is incorporated into ZnO to narrow the bandgap and reduce the recombination rate of the charge carriers (photogenerated electron–hole pairs) on the bare ZnO nanomaterials, as well as create hybrid materials with stronger antibacterial properties expanding the antibacterial activities into a wider variety of practical applications.[10–13] Recently, much attention has been devoted to developing various Ag/ZnO nanomaterials in terms of morphology,[14] size, component, and structure through a series of different synthesis methods, such as the sol–gel method,[10] chem-hydrothermal method,[3–5,15–17] bio-hydrothermal method,[8,12,13] UV-decomposition process,[11] and mechanosynthesis.[18] Almost all of them display impressive enhancements in photocatalytic performance toward toxic organic compounds and antibacterial

[a]*Phenikaa University Nano Institute (PHENA), PHENIKAA University, Hanoi 12116, Vietnam. E-mail: nhung.phamthituyet@phenikaa-uni.edu.vn; tuan.leanh@phenikaa-uni.edu.vn*

[b]*Department of BioNano Technology, Gachon University, 1342 Seongnam-Daero, Sujeong-Gu, Seongnam-Si, Gyeonggi-do 13120, Republic of Korea*

[c]*Faculty of Biotechnology, Chemistry and Environmental Engineering, PHENIKAA University, Hanoi 12116, Vietnam*

[d]*Faculty of Materials Science and Engineering, PHENIKAA University, Hanoi 12116, Vietnam*

[e]*Graduate University of Science and Technology (GUST), Institute for Materials Science (IMS), Vietnam Academy of Science and Technology, 18 Hoang Quoc Viet, Hanoi 10000, Vietnam*

† Electronic supplementary information (ESI) available. See DOI: 10.1039/d1ra08365a

activity. More interestingly, magnesium aminoclay (MgAC) has been demonstrated as a layered synthetic structure possessing many unique features with a large number of amine functional groups, two-dimensional structure, large surface area, high adsorption capacity, non-toxicity, biodegradability, and good dispersion in water.[19] The utilization of MgAC as an effective adsorbent for removing heavy metals and organic dyes as well as a great stabilizer and remarkable surfactant to metal oxide NPs has been investigated in some recent reports. The combination of MgAC and other nanomaterials for environmental treatment purposes in the first step showed positive responses in both adsorption performance, stability, and reusability.[19–23] In such cases, MgAC with amine functional groups, which acted as interaction sites with other nanomaterials, significantly increased loading efficiency, a homogeneous dispersion, and created many individual active sites, avoiding agglomeration, and ensuring long-term structural stability.[24,25]

In this work, a simple two-step electrochemical method using MgAC as a great stabilizer and reductant is introduced for the first time, facilitating the better uniform formation and long-term stability of Ag@ZnO nanoparticles (NPs) on the MgAC matrix without using any chemical additives. The influence of the appearance of both Ag and MgAC on the photocatalytic performance toward methylene blue (MB) degradation and antibacterial activity *via* the strong interaction among ZnO and metallic Ag for both *Salmonella* (*Sal*) and *Staphylococcus aureus* (*S. aureus*) bacterial strains was investigated. The obtained results showed that adding Ag and MgAC not only led to enhanced visible light absorbability and MB degradation performance but also exhibited great antibacterial activity. A possible mechanism for the enhancement of degradation performance and antibacterial activity of Ag@ZnO/MgAC nanocomposites was proposed and discussed.

2. Materials and methods

2.1 Materials

Two pure silver bars and two zinc bars with heights of 10 and 15 cm and thicknesses of 2 and 5 mm were used as working electrodes in the electrochemical processes, respectively. Acetic acid (CH_3COOH, 99.5%) and methylene blue (MB) were provided from Xilong Scientific Co. Ltd. Magie chloride ($MgCl_2 \cdot 6H_2O$, 99%), APTES (3-aminopropyltriethoxysilane, $H_2N(CH_2)_3Si(OC_2H_5)_3$, MW = 221.37, ≥98%), and ethanol (EtOH) were acquired from Shanghai Chemical Reagent. All chemicals used in this work were of reagent grade. In addition, the double-distilled water used in the whole process was purified using a Milli-Q® system (18.2 MΩ cm at 25 °C).

2.2 Synthesis of Ag@ZnO/MgAC

Firstly, Mg-aminoclay (MgAC) was prepared following a procedure similar to our previous reports.[19,22,23] Briefly, 400 mL EtOH solution (94%) was poured in a 500 mL glass beaker, then, 13.2 g of $MgCl_2 \cdot 6H_2O$ was added and completely dissolved for 15 min under magnetic stirring. Next, 23.5 mL of APTES was added dropwise and stirred overnight. The precipitated product was centrifuged and dried at 60 °C for 24 hours. The final product was powdered using a mortar and pestle and used as the pre-precursor in the next experiments.

450 mL of a solution containing 0.5 M acid acetic was prepared in a 500 mL glass beaker. Two bare Zn bars as the cathode and anode were immersed in this glass beaker with a depth of about 10 cm and spaced at 7 cm. A DC voltage source of 20 V was applied to electrodes. The electrochemical process was carried out for 2 hours at room temperature without using any chemical additives. Then, the final solution was magnetically stirred under ambient conditions for 30 min. Next, the electrolysis process of bare Ag bars was also set up similarly to the above experiment in the obtained electrolysis solution. However, herein the supplied voltage was around 10 V for 15 min. After the electrochemical process was completed, a determined amount of the prepared MgAC (0, 2.25, 4.5, and 9 g) was added to this electrolysis solution and stirred at various temperatures (25 °C, 40 °C, and 70 °C) for 1 hour as described in Table 1, respectively. During stirring, the color of the solution gradually changed from transparent to purplish brown, suggesting the formation of Ag@ZnO/MgAC nanocomposites (Fig. 1).

2.3 Material characterization

The crystalline characterization and structural properties of Ag@ZnO/MgAC nanocomposites were investigated and analyzed using X-ray diffraction (XRD) with Cu Kα radiation at 40 keV and 40 mA and Raman spectroscopy (Macro Ram, Horiba Scientific). The morphology, size, distribution, and preferential orientation of the materials were observed using a scanning electron microscope (SEM, HITACHI, S-4800-3000F). Further, the elemental composition of Ag@ZnO/MgAC nanocomposites was performed using X-ray fluorescence (XRF)

Table 1 List of as-prepared samples for studying photocatalytic and antibacterial activities

Samples	Weight percent of added MgAC (wt%)	Electrolysis time of Zn bars (min)	Weight percent of Zn (wt%)	Electrolysis time of Ag bars (min)	Weight percent of Ag (wt%)	Treatment temperature (°C)
S0	0	120	1.77	30	0.27	Room temp.
S1	10	120	1.62	30	0.29	Room temp.
S2	10	120	1.79	30	0.34	40
S3	10	120	1.51	30	0.34	70
S4	20	120	1.66	30	0.39	40
S5	5	120	1.55	30	0.38	40

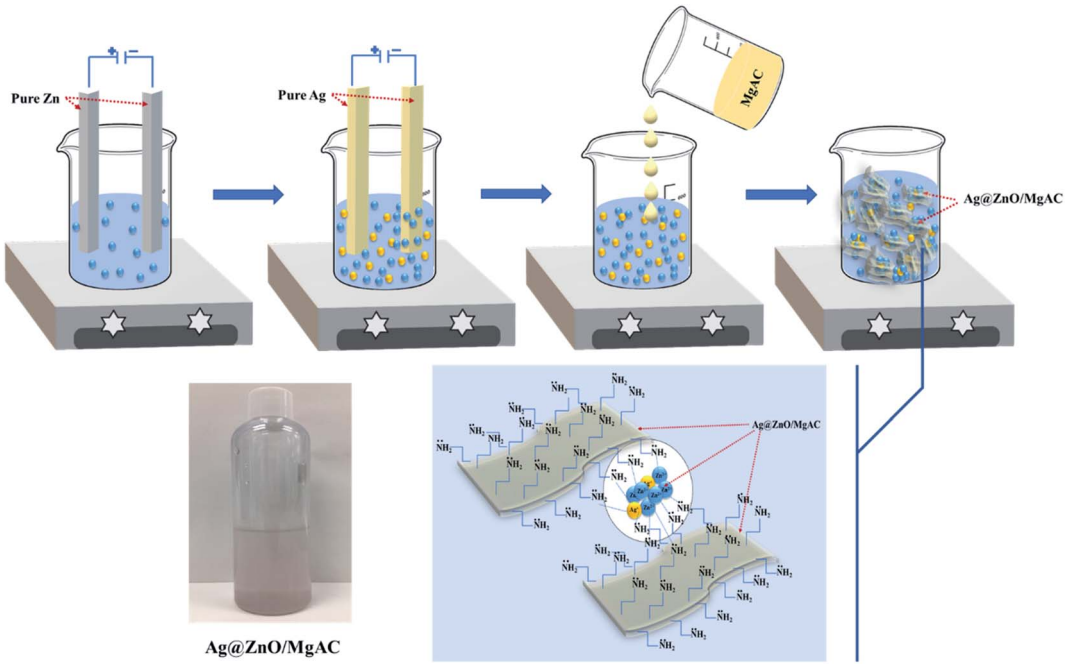

Fig. 1 Schematic illustrations for the synthesis of Ag@ZnO/MgAC nanocomposite design using the electrochemical method.

spectrophotometry (MiniPal 2, PANalytical, Netherlands). More particularly, UV-vis spectroscopy (HITACHI U-3900) was used to determine the bandgap as well as evaluate the photocatalytic properties of Ag@ZnO/MgAC.

2.4 Photocatalytic test

The photocatalytic activity of the as-prepared samples was determined by investigating the decomposition of MB as a target pollutant under visible light irradiation. Firstly, 5 mL of the catalyst solution was added to 50 mL of MB aqueous solution (150 ppm); this suspension was continuously stirred under a magnetic stirrer in the dark to reach equilibrium adsorption between the photocatalyst surface and MB molecule. Next, a 50 W incandescent lamp with the main wavelength in the range from 400 to 720 nm was used as the visible light source for the photocatalysis process. After a given irradiation time, about 4 mL of the mixed solution was withdrawn and centrifuged to separate the catalysts from the mixed solution. The photodegradation of MB solution was monitored by measuring the intensity of the absorption peak at 665 nm using UV-vis spectroscopy. Comparative experiments of MB degradation using a control sample (0.5 M acid acetic), Ag@ZnO sample, and Ag@ZnO/MgAC samples with various MgAC amounts and treated temperatures were also performed. The degradation efficiency of MB was calculated according to the following formula: degradation (%) = $(Abs_t/Abs_0) \times 100$; where Abs_0 is the initial absorbance and Abs_t is the absorbance at "t" time.

2.5 Photoelectrochemical test

To evaluate the photoelectrochemical behavior of Ag@ZnO/MgAC, electrochemical impedance spectroscopy (EIS) and linear sweep voltammetry (LSV) measurements were carried out on the Palmsens 4 electrochemical workstation at ambient atmosphere with and without visible light irradiation in 0.1 M KCl solution. Firstly, the commercial carbon screen-printed electrodes (SPEs-DS110) were modified by Ag@ZnO/MgAC, acted as a working electrode during testing. For EIS measurement, the frequency range was 100 kHz to 50 mHz with an applied ac potential of −0.2 V. Besides, LSV measurement was performed at a scan rate of 50 mV s^{-1} with the potential range from −1 V to −0.2 V.

2.6 Antibacterial test

Antibacterial activity of the as-synthesized samples with different concentrations was analyzed against selected Gram-negative *E. Salmonella enteritidis* WHO 2013 S13.3 (*Sal*) and Gram-positive *Staphylococcus aureus* ATCC 25923 (*S. aureus*) using the agar well diffusion method. The antimicrobial activity was performed by spreading about 100 μL ($1–2 \times 10^8$ CFU mL^{-1}) of each bacterial culture over the entire agar plate surface by a sterile glass spreader. Then, the holes with 8 mm diameter were created in the agar discs with a sterile cork borer. 50 μL of the suspension of the as-synthesized samples with desired concentrations was introduced into the well. Moreover, 0.5 M acid acetic was used as a control sample. Then, these plates were cultured in a 37 °C incubator for 24 hours. The antibacterial properties of the synthesized samples were assessed by observing and measuring the diameter of the inhibition zone against the bacteria.

3. Results and discussion

3.1 Characterization of Ag@ZnO/MgAC

As observed in XRD patterns of ZnO/MgAC and Ag@ZnO/MgAC samples (Fig. 2c), the appearance of characteristic peaks at

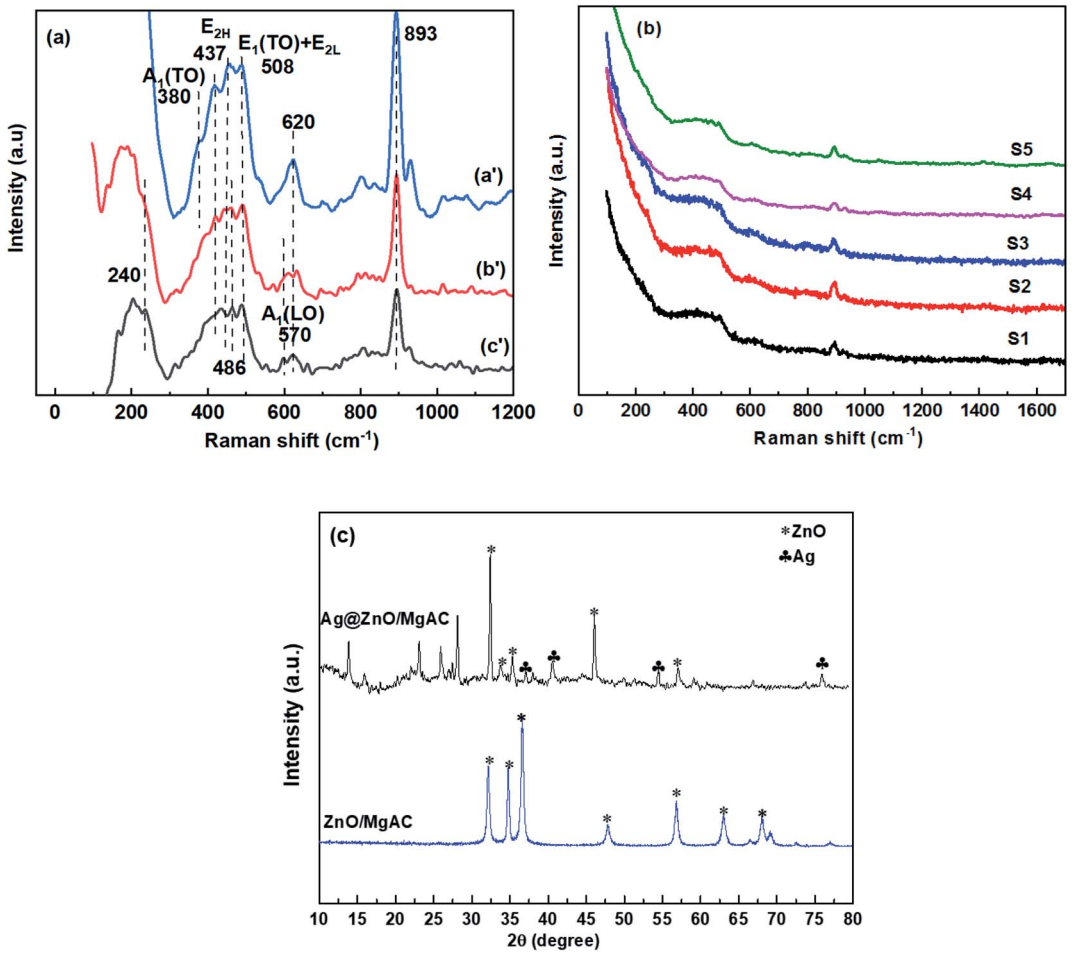

Fig. 2 (a and b) Raman spectra of ZnO/MgAC (a′), Ag@ZnO (b′), and the different Ag@ZnO/MgAC (c′) samples synthesized at various conditions; (c) XRD results of ZnO/MgAC and Ag@ZnO/MgAC samples.

31.7°, 34.4°, 36.2°, 47.5°, and 56.6° in both samples was well indexed to (100), (002), (101), (102), and (110) planes, respectively, of hexagonal wurtzite structure of ZnO (JCPDS standard card no. 36-1451). Besides, the other diffraction peaks were also found at around 37.2°, 40.5°, 54.8°, and 76.1°, suggesting the formation of Ag according to JCPDS (87-0598) within the Ag@ZnO/MgAC crystalline lattice structure. More particularly, there were remarkable changes recorded either in the diffraction intensity and position of ZnO lattice in the presence of Ag. Namely, the diffraction intensity of characteristic (100) and (102) planes in the ZnO lattice remarkably increased, meanwhile, other characteristic peaks seem to decrease. Furthermore, these main diffraction peaks tended to shift toward the higher angle upon Ag incorporation, revealing a decrease of crystallinity of ZnO lattice as well as the incorporation of Ag^+ ions into the ZnO structure, in agreement with previous reports in the literature.[5,11,26–28] It is worth mentioning that the diffusion of Ag^+ ions into the ZnO lattice has been demonstrated to be preferred to substitute Zn^{2+} ions on the surface of the ZnO phase more than into O sites because the surface defects not only can act as dangling bonds but also possess a proper energy level to trap the ionic doping.[11] Furthermore, the diffusion of Ag^+ ions could be difficult to lead to interstitial sites of Zn^{2+} ions. Unfortunately, the incorporeality of Ag^+ ions in the ZnO structure still achieved a low efficiency, explained *via* the appearance of small and weak diffraction peaks in Ag@ZnO/MgAC nanocomposites. The reason for this limitation was explained in that the reaction solution just contained a small weight percentage of Zn and Ag (approximately 1.65% and 0.34%), corresponding to a low proportion of approximately 0.2 between Ag and Zn within the Ag@ZnO/MgAC nanocomposites, which was determined from XRF results (Table 1 and Fig. S1†). More importantly, the large difference in ionic radii of Ag^+ (1.26 Å) and Zn^{2+} (0.74 Å) inhibited the incorporeality efficiency of Ag^+ ions in the ZnO structure.[1,11,26] Herein, the formation process of Ag@ZnO/MgAC nanocomposites could be described as follows:

After the electrochemical process of two pure Zn bars was completed, the obtained electrolysis solution contained ZnO NPs arising from the self-reduction process at the cathode surface and a large number of residual Zn^{2+} ions under ambient conditions. During the next electrochemical process involving two Ag bars, a part of the residual Zn^{2+} ions was attracted to the cathode surface along with the created Ag^+ ions. Besides, the formation of Ag nanoclusters on the ZnO surface

contemporaneously started. A final electrolysis solution included residual Zn^{2+}, Ag^{+} ions, and Ag@ZnO nanoparticles. The formation of Ag@ZnO NPs actually became stronger and more homogenous after adding layered MgAC, a Lewis base with amine functional groups. Namely, MgAC could donate free electrons to the reduction process of both Ag^{+} and Zn^{2+} ions in the electrolysis solution. The simultaneous growth of crystalline phases of ZnO and Ag on the MgAC matrix led to the diffusion of foreign ions into their lattice that is inevitable. This formation mechanism further confirmed the incorporation of Ag^{+} ions in the ZnO structure. These results demonstrated a clear and distinct formation of Ag@ZnO NPs in the MgAC matrix, indicating good synthesis of nanocomposites.

To further evaluate the crystalline quality and formation of Ag@ZnO/MgAC nanocomposites, the Raman analysis of ZnO/MgAC, ZnO@Ag, and Ag@ZnO/MgAC samples at different experimental conditions as described in Table 1 was performed (Fig. 2a and b). Firstly, for the ZnO/MgAC sample, the Raman spectrum showed three peaks centered at 380, 437, and 508 cm^{-1}, which were considered to be the vibration modes A_1 transversal optical (A_1(TO)), E_2 high (E_{2H}), and E_1(TO) + E_{2L}, respectively.[3,5,26] The clear observation of these peaks correlated with the vibration of Zn atoms in the ZnO wurtzite lattice structure, suggesting the high crystallization of the ZnO. Besides, the appearance of the peaks located at about 620 and 893 cm^{-1} was detected in all three samples ZnO/MgAC, Ag@ZnO, and Ag@ZnO/MgAC, revealing the existence of acetic acid molecules in the sample solution. After the addition with low content of Ag, detectable changes in the intensity and location of A_1(TO) and E_{2H} modes of hexagonal ZnO in both Ag@ZnO and Ag@ZnO/MgAC samples were observed. Namely, A_1(TO) and E_{2H} peaks were drastically decreased in intensity along with shifting towards lower energy due to Zn–Ag bonds, low crystallinity, and the breakdown of translational crystal symmetry by the incorporated defects and impurity in the ZnO lattice after Ag incorporation.[26,27] More interestingly, Raman spectra of Ag@ZnO and Ag@ZnO/MgAC samples showed some new peaks centered at around 240, 486, and 570 cm^{-1}. In which, the peak centered at 570 cm^{-1} could be assigned to the broadened A_1(LO) phonon mode, assigned to the oxygen vacancies, zinc interstitials, and/or defect complexes in the ZnO crystal,[3,29] while, the peak at about 486 cm^{-1} was assigned as the interfacial surface phonon mode as mentioned in the literature related to doping of other metals (Mn, Co) in the ZnO lattice.[26,28] Another anomalous vibrational mode appeared at about 240 cm^{-1}, which has also been reported for ZnO doped with some other elements and could be associated with the lattice-host intrinsic defects created by the doping or the local vibrations of Ag atoms in the ZnO lattice.[26–28,30] Particularly, the appearance of these new peaks was more easily observed in the Ag@ZnO–MgAC sample, revealing the effective support of the MgAC matrix in enhancing the formation of Ag@ZnO NPs. Clearly, these obtained results are in agreement with the above XRD analysis. In a comparison among Ag@ZnO/MgAC samples prepared at different experimental conditions (treatment temperature and MgAC content), Raman spectra of all samples still exhibited characteristic phonon modes of hexagonal ZnO lattice and Ag atoms, however, the diffraction intensity and width of these Raman peaks had significant differences. Among them, the Ag@ZnO/MgAC sample prepared at 40 °C and that containing 10% MgAC (wt%) (sample S2) displayed a high peak intensity, along with the strongest and sharpest Raman peaks, suggesting highly crystalline nature, structural stability, as well as proper proportion among components within Ag@ZnO/MgAC nanocomposites. Hence, sample S2 was chosen as an optimal sample for the next experiments.

The formation of Ag@ZnO NPs on the MgAC matrix also considerably affected the optical properties of nanocomposites, which were evaluated *via* UV-vis diffuse absorption spectra of ZnO/MgAC, Ag@ZnO, and Ag@ZnO/MgAC samples in the 200–700 nm wavelength range as shown in Fig. 3. As can be seen, both ZnO/MgAC, Ag@ZnO, and Ag@ZnO/MgAC exhibited strong absorption in the UV light range. Namely, ZnO/MgAC possessed a maximum absorption peak at around 350 nm, corresponding to a bandgap value of 3.23 V. However, by adding Ag, the light absorption of Ag@ZnO and Ag@ZnO/MgAC samples within the visible region was significantly improved as described by the shift towards longer wavelength and

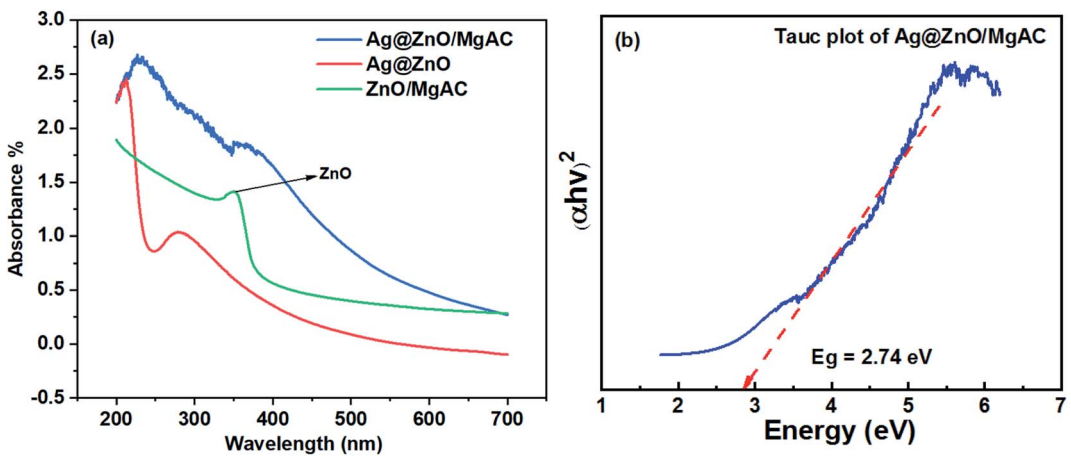

Fig. 3 (a) UV-Vis absorption spectrum of ZnO/MgAC, Ag@ZnO, and Ag@ZnO/MgAC nanocomposites; (b) energy band gap estimation through the results of the Tauc plot of Ag@ZnO/MgAC.

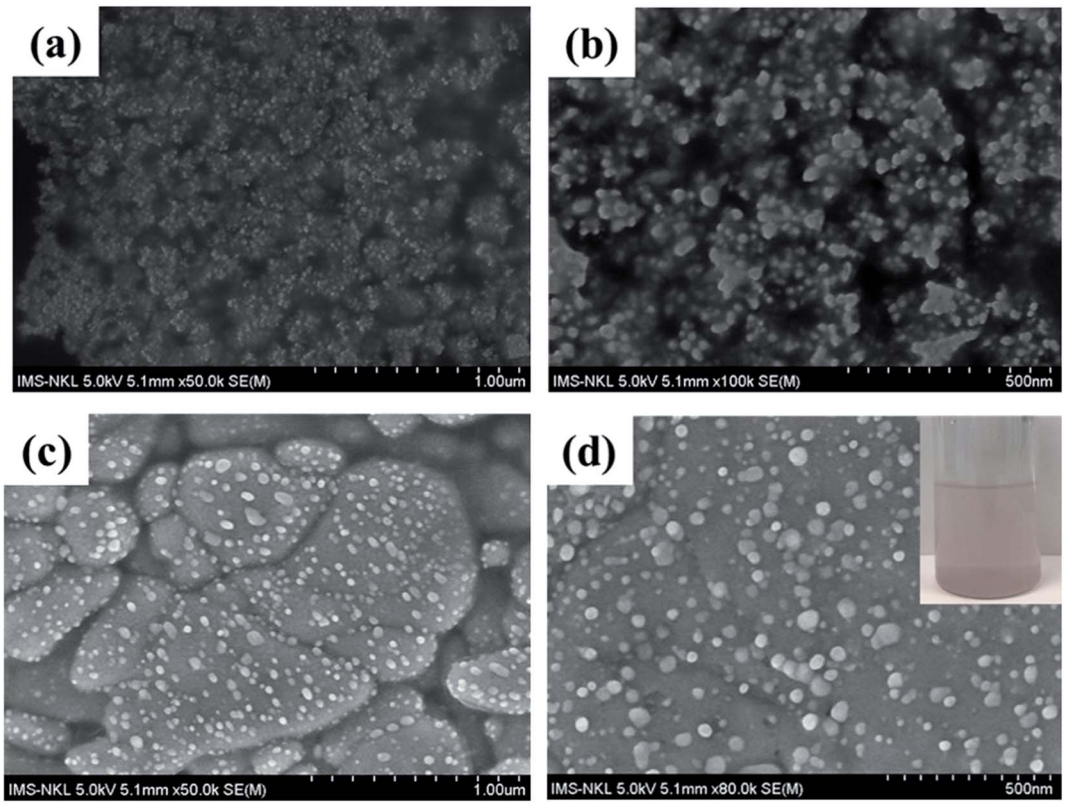

Fig. 4 SEM images of the synthesized Ag@ZnO samples (a and b); and Ag@ZnO/MgAC sample (c and d). The inset of (d) shows Ag@ZnO/MgAC sample image after storing for 3 days.

stronger absorption intensity over the range from 400 to 700 nm, corresponding to a lower bandgap value of 2.74 V for the Ag@ZnO/MgAC sample. More interestingly, it seems that a positive shift of the wavelength and the increase in the absorption intensity of the visible light region occurred more strongly in the Ag@ZnO/MgAC sample. This further demonstrated the important role of MgAC and Ag in enhancing the formation as well as the optical properties of nanocomposites. To explain the broadened absorption in the visible region, some possible reasons are proposed. As described above, the incorporation of Ag^{+} ions in the ZnO structure on the MgAC matrix surface can cause an increase in a large number of lattice defect sites. Such defect sites act as trapping sites for the electrons in the crystalline structure, inhibiting the unwanted recombination rate of the photogenerated charge carriers and promoting more efficient separation of electron–hole pairs, leading to prolonging their lifetime.[2,26] Besides, benefiting from the surface plasmon resonance (SPR) effect, Ag can considerably enhance the absorption performance of visible light,[3,14] resulting in the visible light effective absorption capacity of Ag@ZnO/MgAC nanocomposites. Furthermore, the energy band matching of ZnO and Ag function ranges also accelerates the light absorption capacity.

To further investigate the formation and surface morphology of Ag@ZnO NPs in the prepared samples, SEM images were recorded and are shown in Fig. 4. The particle size of the formed spherical Ag@ZnO NPs in both samples was about 50–100 nm. It is interesting to note that most of the Ag@ZnO NPs tended to be aggregated with each other in the absence of the MgAC matrix. By adding MgAC, Ag@ZnO NPs still maintained their morphology, however, the dispersion of Ag@ZnO NPs in MgAC seemed to be more homogeneous. The effective distribution of Ag@ZnO/MgAC also was investigated in the solution. By storing the Ag@ZnO/MgAC solution samples for 3 days, no aggregation phenomenon of Ag@ZnO NPs was observed in this case. In some of our previous reports, it was demonstrated that MgAC nanomaterials could enhance the great water dispersibility of metal and metal oxide NPs owing to their amine functional groups. Furthermore, the connection between the nanoparticles and MgAC is strong because nanoparticles cannot be separated from the aminoclay matrix.[19,23,31] This measurement further confirms the uniform formation of Ag@ZnO NPs on the surface of the MgAC matrix.

3.2 Photocatalytic activity of Ag@ZnO/MgAC nanocomposites

The photodegradation performance of Ag@ZnO/MgAC samples prepared under various conditions (treatment temperature and MgAC content), ZnO/MgAC, Ag@ZnO, and control sample (acid acetic) for MB under visible light irradiation as the model reaction was measured (Fig. 5) using UV-vis measurements. As illustrated in Fig. 5a, the absorption peak at 665 nm ascribed to MB was rapidly reduced with the increase of irradiation time. The photodegradation efficiency showed that compared to the control sample, Ag@ZnO/MgAC possessed higher

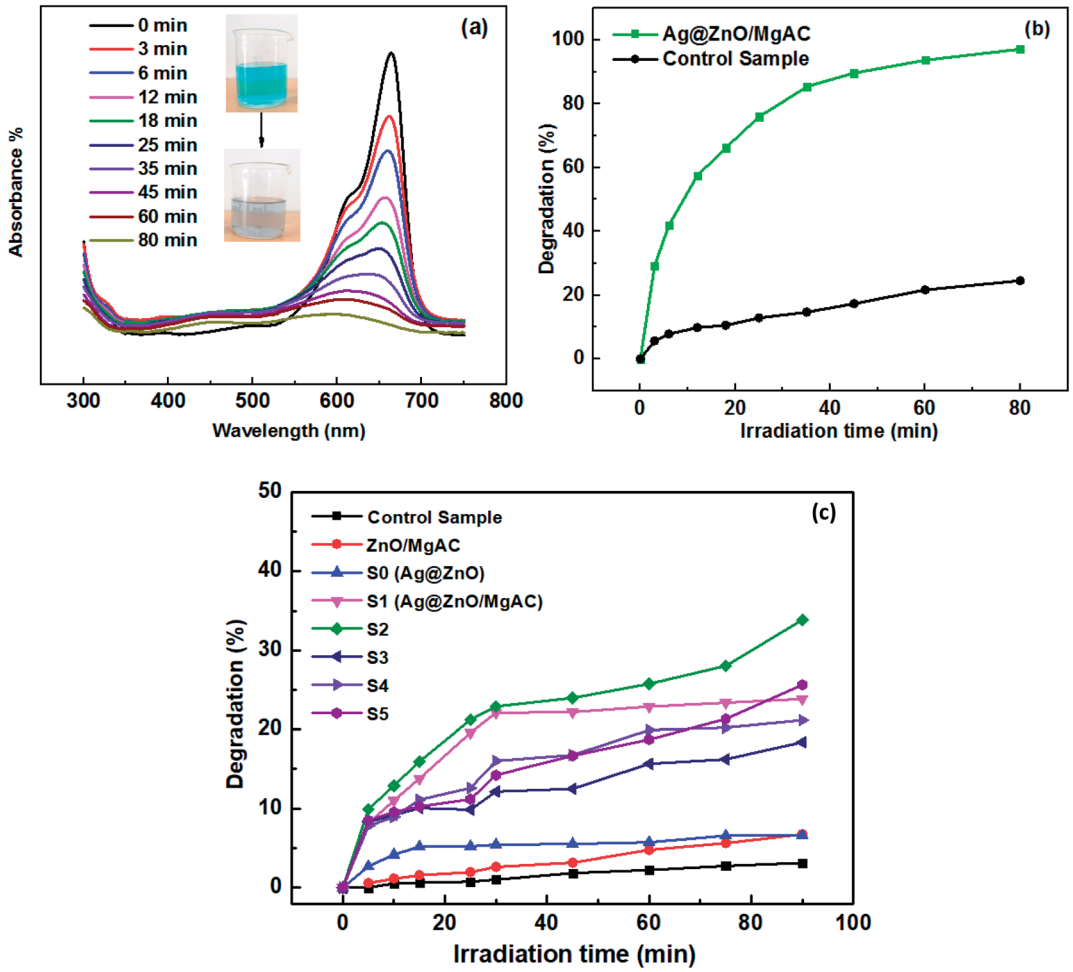

Fig. 5 (a and b) The MB (50 ppm) degradation efficiency in the presence of the ZnO@Ag/MgAC and control samples under visible light irradiation; (c) the comparison of the photocatalytic degradation of MB (150 ppm) by ZnO/MgAC, Ag@ZnO (S0), various Ag@ZnO/MgAC samples (S1, S2, S3, S4, and S5), and no photocatalyst control sample under visible light irradiation.

photocatalytic activity for MB degradation under visible light irradiation due to the charge separation and visible light-harvesting properties of Ag@ZnO NPs. Indeed, almost all MB molecules (98.7%) were completely degraded after 80 min under visible light irradiation in the presence of the Ag@ZnO/MgAC photocatalyst, in contrast, the self-degradation of MB at

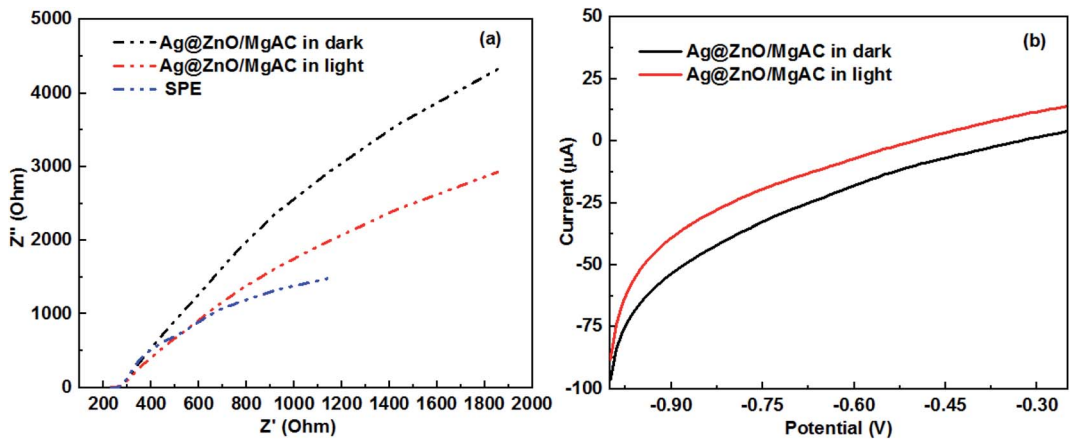

Fig. 6 (a) Nyquist plots of SPE and Ag@ZnO/MgAC/SPE electrodes and (b) linear scan voltammograms obtained for Ag@ZnO/MgAC/SPE electrodes under dark and visible light irradiations.

the same condition was just less than 25%. More interestingly, in another comparison among Ag@ZnO/MgAC samples and ZnO/MgAC, even the Ag@ZnO sample (without MgAC in the synthetic process), the highest observed photocatalytic activity of Ag@ZnO/MgAC treated at 40 °C (sample S2) demonstrated that adding a suitable content of MgAC and Ag within nanocomposites was critically important because it significantly impacted the photocatalytic activity (Fig. S2†).

In this case, MgAC not only played the role of the Lewis base, which could donate a pair of electrons to Ag^{+} and Zn^{2+} ions on its surface to promote the reduction of these ions and then form Ag@ZnO NPs, but also as a great stabilizer in the matrix with a large number of active amino functional groups, facilitating the uniform distribution and preventing self-aggregation of Ag@ZnO NPs. Furthermore, this result indicated that the formation of Ag@ZnO/MgAC nanocomposites occured better at 40 °C because the increase in temperature can result in an increase in size and cause crystal growth, which causes aggregation and low degradation performance towards MB. Besides, the excessive addition of MgAC brings down photocatalytic performance due to the large wrapping surface and the too thick coating of MgAC on the Ag@ZnO active material, leading to the reduced exposure area and absorption surface, as well as the interaction ability between MB and active material. This result was also consistent with the obtained Raman spectrum of Ag@ZnO/MgAC at 40 °C with the high crystalline quality seen from clearer and stronger peaks.

With the presence of Ag within the ZnO/MgAC sample, the mechanism for MB degradation could be proposed based on the basis of photoexcitation of Ag@ZnO/MgAC nanocomposites. When the incident visible light excites the carriers in Ag@ZnO nanostructures, owing to strong surface plasmon resonance (SPR) and energy band matching of Ag with ZnO, electron–hole pairs are created in Ag atom sites. These photoexcited electrons can escape more easily from Ag ions than from the Zn ions and then transfer to the conduction band (CB) of

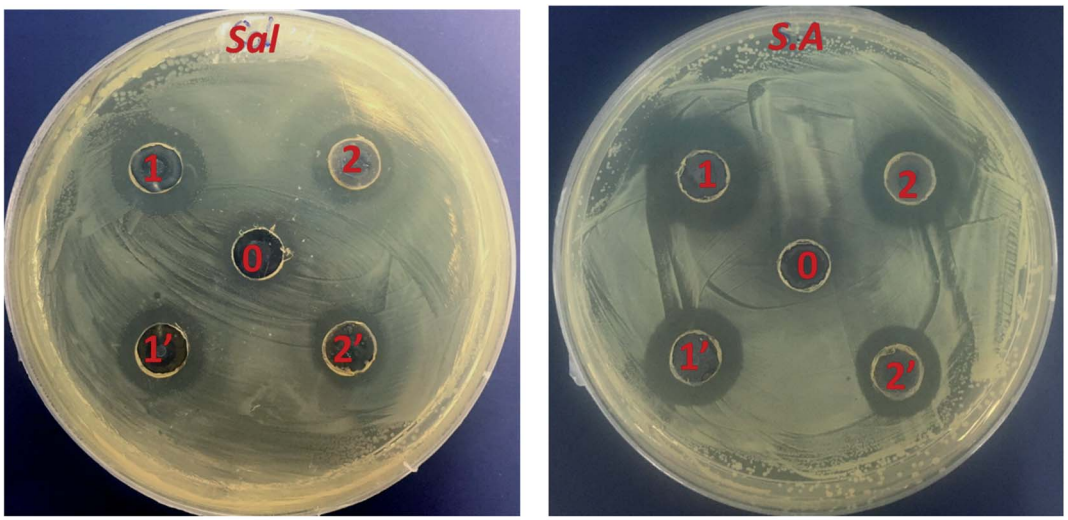

Samples	Inhibition zone (mm)	
	Sal	*S. aureus*
Control Sample	0	0
Ag@ZnO (C_o M)	16	20
Ag@ZnO ($C_{o/2}$ M)	15	17
Ag@ZnO/MgAC (C_o M)	14	17
Ag@Zn/MgAC ($C_{o/2}$ M)	13	15

Fig. 7 Inhibition zone of Ag@ZnO/MgAC, Ag@ZnO at various concentrations (C_o, $C_{o/2}$), and the control sample (acid acetic) on *Salmonella enteritidis* (*Sal*) and *Staphylococcus aureus* (*S.A.*) bacteria.

ZnO because the work function of Ag is lower 4.26 eV than that of ZnO (5.2 eV) until the two levels reach equilibrium and form a new Fermi energy level, that is more positive than the conduction band of bare ZnO.[11,14,17,28] On the one hand, herein, the CB of ZnO acts as an electron well to collect and gather the photoexcited electrons from Ag atoms sites by the electron sink effect. The various reactive oxygen species and hydroxyl radicals such as $^{\bullet}O^{2-}$, $^{\bullet}OH$, and/or $^{\bullet}OOH$ are created by the interaction between the transferred electrons and dissolved oxygen molecules in water, then they directly degraded MB molecules.[3,32] In addition, the photoexcited holes in Ag atom sites directly oxidize MB molecules, leading to increased photocatalytic performance. On the other hand, the next effective charge separation and transfer of the photoexcited electrons can transfer from the conduction band of the Ag@ZnO to the Femi level of bare ZnO NPs, which is attributed to remarkably refrain the recombination and lengthen the lifetime of the photogenerated electron–hole pairs, improving the photocatalytic activity of Ag@ZnO/MgAC nanocomposites.[2,11]

To obtain further insight into the interface charge separation efficiency of the photogenerated electrons and holes in promoting the photocatalytic activity of Ag@ZnO/MgAC nanocomposites, EIS measurements were performed in 0.1 M KCl electrolyte solution. As we know, based on EIS Nyquist plots, the arc radius is a crucial value that presents the interface layer resistance (R_{ct}) occurring at the electrode surface, according to that, a smaller arc radius implies a higher transferability and better separability of photogenerated electron–hole pairs from the electrode material.[2,15,32] Fig. 6a shows EIS Nyquist plots of electrodes modified with Ag@ZnO/MgAC under dark and visible light irradiation. Clearly, the modification with Ag@ZnO/MgAC resulted in a higher separation and transport efficiency reflected by a decrease in the plot radius than that of the pure SPE, both with and without light irradiation. Furthermore, the visible light response of Ag@ZnO/MgAC nanocomposites *via* LSV measurements in dark and under visible light irradiation was investigated as shown in Fig. 6b. Herein, the obtained photocurrent of the Ag@ZnO/MgAC-based electrode was enhanced under visible light irradiation, demonstrating effective improvement in its photoconversion efficiency.[32] It was also an ideal proof showing the enhancement of charge transport rate and the effective separation of electron–hole pairs within Ag@ZnO/MgAC nanocomposites.

3.3 Antibacterial activity of Ag@ZnO/MgAC nanocomposites

As demonstrated in some previous reports, ZnO NPs showed an effective antibacterial activity *via* the formation of reactive oxygen species (ROS) and the release of Zn^{2+}. Therefore, the antibacterial activity of Ag@ZnO and Ag@ZnO/MgAC was studied *via* the evaluation of the inhibition zone against two experimental bacterial strains (*Sal* bacteria and *S. aureus* bacteria) using the agar well diffusion test as shown in Fig. 7. As expected, the control sample (acid acetic) did not show any antimicrobial effect. More interestingly, the antibacterial efficacy shows a marked dependence on the concentration and component of introduced material into each agar disc. Overall, Ag@ZnO and Ag@ZnO/MgAC samples had a clear inhibition zone, however, the size of the inhibition zone of Ag@ZnO in both bacterial strains was significantly larger than that of Ag@ZnO/MgAC, suggesting better antimicrobial activity of Ag@ZnO NPs. A similar trend was observed when the concentration of the introduced materials was reduced in half part. This is possibly explained as suitable because the MgAC matrix played a role as a great stabilizer to hindering exposure of Ag@ZnO NPs to the microbial cell membrane as well as the liberation of Ag^{+} and Zn^{2+} ions from the nanocomposite surface. However, the antibacterial properties of Ag@ZnO/MgAC were still impressive against the two bacterial strains that were studied, providing further evidence for the effective incorporation of Ag@ZnO as well as the synergistic effect among the Ag@ZnO NPs and MgAC.

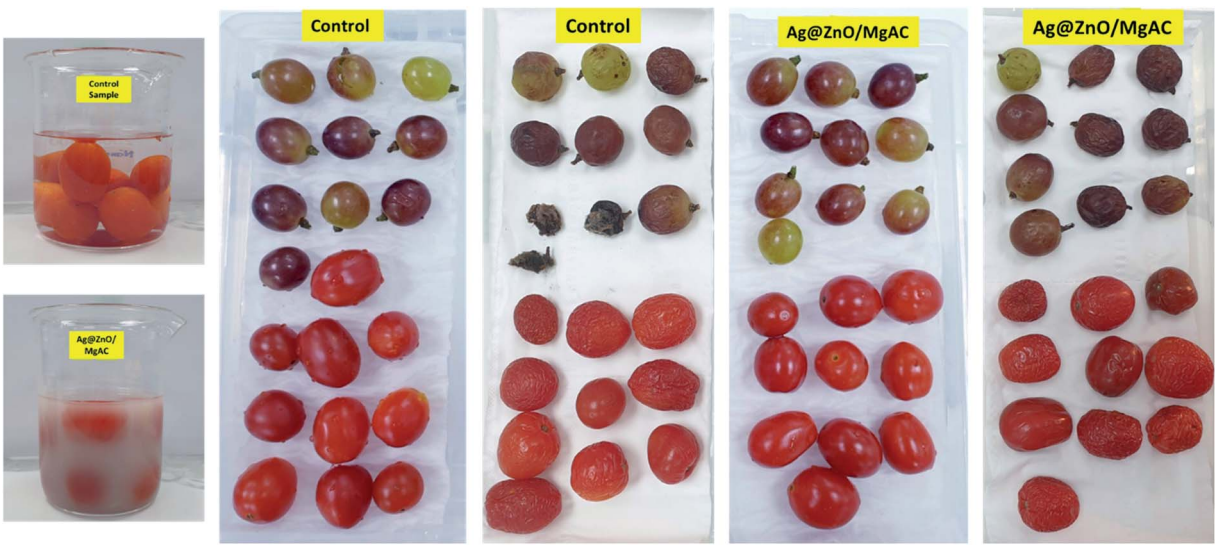

Fig. 8 Antimicrobial activity of Ag@ZnO/MgAC and control samples on real samples (grape and tomato) after 7 days.

In another experiment, the antimicrobial activities of Ag@ZnO/MgAC and control samples were tested on various real samples using grapes and tomatoes and then were observed during the seven days of storage. As can be seen in Fig. 8, grape and tomato samples were immersed in the Ag@ZnO/MgAC solution for 10 min and stored at room temperature for seven days, with no spoilage or microorganism invasions such as fungi and bacteria were observed. Differing from this phenomenon, for the control sample, the grape sample was rapidly decayed and spoiled when not refrigerated, revealing the promising practical application potential of Ag@ZnO/MgAC in food storage fields.

4. Conclusions

Ag@ZnO/MgAC photocatalysts were synthesized by a simple two-step electrochemical method with the addition of MgAC. It was found that the diffusion of Ag atoms into the ZnO crystal structure promoted the absorption capacity of the visible-light region and inhibited unwanted electron–hole recombination owing to the strong SPR effect of Ag and energy band matching between ZnO and Ag. The formation of Ag@ZnO/MgAC nanocomposites was attributed to being beneficial to the enhancement of the degradation efficiency of MB under visible light irradiation as well as antibacterial activity against both two Gram-negative *Sal* and Gram-positive *S. aureus* bacterial strains. As a result, the photodegradation efficiency of MB of the Ag@ZnO/MgAC photocatalyst under visible light irradiation was rather high, approximately 98.56% for 80 min. Furthermore, the antibacterial properties of Ag@ZnO/MgAC nanocomposites were very impressive, exhibiting a large size of the inhibition zone in the agar well diffusion test owing to the synergistic effect among Ag@ZnO NPs and MgAC.

Author contributions

Tuyet Nhung Pham and Anh-Tuan Le conceptualized the project, directed the study. Tuyet Nhung Pham and Nguyen Thi Hue carried out the experimental methods, completed the pre-experiment, analyzed, discussed the results, as well as wrote the manuscript. Tran Dang Thanh and Vu Dinh Lam performed most of the experiments and characterization techniques. Tran Quang Huy and Nguyen Thi Thu Thuy organized the ESI.† Young-Chul Lee, Hoang Van Tuan, Nguyen Tien Khi, and Vu Ngoc Phan contributed equally to this work. Anh-Tuan Le acquired funding for the whole study. All authors commented on the manuscript.

Conflicts of interest

The authors declare that they have no known competing financial interests or personal relationships that could have appeared to influence the work reported in this paper.

Acknowledgements

This research was supported by the Vietnam National Foundation for Science and Technology Development (NAFOSTED) through a fundamental research project (103.02-2018.50). The authors would like to acknowledge the support from NEB Lab at the Phenikaa University for electrochemical, Raman, UV-vis measurements.

References

1 A. E. Ramirez, M. Montero-Munoz, L. L. Lopez, J. E. Ramos-Ibarra, J. A. H. Coaquira, B. Heinrichs and C. A. Paez, Significantly enhancement of sunlight photocatalytic performance of ZnO by doping with transition metal oxides, *Sci. Rep.*, 2021, **11**(1), 2804.

2 Y. Wang, Y. Z. Zheng, S. Lu, X. Tao, Y. Che and J. F. Chen, Visible-light-responsive TiO_2-coated ZnO: I nanorod array films with enhanced photoelectrochemical and photocatalytic performance, *ACS Appl. Mater. Interfaces*, 2015, **7**(11), 6093–6101.

3 T. Mahardika, N. A. Putri, A. E. Putri, V. Fauzia, L. Roza, I. Sugihartono and Y. Herbani, Rapid and low temperature synthesis of Ag nanoparticles on the ZnO nanorods for photocatalytic activity improvement, *Results Phys.*, 2019, **13**, 102209.

4 Q. Deng, X. Duan, D. H. Ng, H. Tang, Y. Yang, M. Kong, Z. Wu, W. Cai and G. Wang, Ag nanoparticle decorated nanoporous ZnO microrods and their enhanced photocatalytic activities, *ACS Appl. Mater. Interfaces*, 2012, **4**(11), 6030–6037.

5 O. Bechambi, M. Chalbi, W. Najjar and S. Sayadi, Photocatalytic activity of ZnO doped with Ag on the degradation of endocrine disrupting under UV irradiation and the investigation of its antibacterial activity, *Appl. Surf. Sci.*, 2015, **347**, 414–420.

6 L. Chang, Y. Feng, B. Wang, X. Huang, D.-P. Yang and Y. Lu, Dual functional oyster shell-derived Ag/ZnO/$CaCO_3$ nanocomposites with enhanced catalytic and antibacterial activities for water purification, *RSC Adv.*, 2019, **9**(70), 41336–41344.

7 L. Bai, S. Zheng, Z. Li, X. Wang, Y. Guo, L. Ye and J. Mao, Design of Ag-decorated ZnO concave nanocubes using ZIF-8 with dual functional catalytic ability for decoloring dyes, *CrystEngComm*, 2018, **20**(21), 2980–2988.

8 M. Zare, K. Namratha, S. Ilyas, A. Hezam, S. Mathur and K. Byrappa, Smart Fortified PHBV-CS Biopolymer with ZnO-Ag Nanocomposites for Enhanced Shelf Life of Food Packaging, *ACS Appl. Mater. Interfaces*, 2019, **11**(51), 48309–48320.

9 Y. Deng, L. Yang, X. Huang, J. Chen, X. Shi, W. Yang, M. Hong, Y. Wang, M. S. Dargusch and Z. G. Chen, Dual Ag/ZnO-Decorated Micro-/Nanoporous Sulfonated Polyetheretherketone with Superior Antibacterial Capability and Biocompatibility via Layer-by-Layer Self-Assembly Strategy, *Macromol. Biosci.*, 2018, **18**(7), 1800028.

10 D. Tekin, T. Tekin and H. Kiziltas, Photocatalytic degradation kinetics of Orange G dye over ZnO and Ag/ZnO thin film catalysts, *Sci. Rep.*, 2019, **9**(1), 17544.

11 J. M. Wu and W. T. Kao, Heterojunction Nanowires of $Ag_xZn_{1-x}O$–ZnO Photocatalytic and Antibacterial Activities under Visible-Light and Dark Conditions, *J. Phys. Chem. C*, 2015, **119**(3), 1433–1441.

12 M. Zare, K. Namratha, S. Alghamdi, Y. H. E. Mohammad, A. Hezam, M. Zare, Q. A. Drmosh, K. Byrappa, B. N. Chandrashekar, S. Ramakrishna and X. Zhang, Novel Green Biomimetic Approach for Synthesis of ZnO-Ag Nanocomposite; Antimicrobial Activity against Food-borne Pathogen, Biocompatibility and Solar Photocatalysis, *Sci. Rep.*, 2019, **9**(1), 8303.

13 M. Khatami, R. S. Varma, N. Zafarnia, H. Yaghoobi, M. Sarani and V. G. Kumar, Applications of green synthesized Ag, ZnO and Ag/ZnO nanoparticles for making clinical antimicrobial wound-healing bandages, *Sustainable Chem. Pharm.*, 2018, **10**, 9–15.

14 X. Zhang, Y. Wang, F. Hou, H. Li, Y. Yang, X. Zhang, Y. Yang and Y. Wang, Effects of Ag loading on structural and photocatalytic properties of flower-like ZnO microspheres, *Appl. Surf. Sci.*, 2017, **391**, 476–483.

15 S. Ma, S. Zhan, Y. Xia, P. Wang, Q. Hou and Q. Zhou, Enhanced photocatalytic bactericidal performance and mechanism with novel Ag/ZnO/g-C_3N_4 composite under visible light, *Catal. Today*, 2019, **330**, 179–188.

16 C. Feng, Z. Chen, J. Jing and J. Hou, The photocatalytic phenol degradation mechanism of Ag-modified ZnO nanorods, *J. Mater. Chem. C*, 2020, **8**(9), 3000–3009.

17 S. N. H. Daud, C. Y. Haw, W. S. Chiu, Z. Aspanut, N. A. Jani, P. S. Khiew, Y. C. Lim, M. A. Abd and A. M. A. Hamid, 3D hyperbranched heterostructures of Ag nanocrystals-decorated ZnO nanopillars: controlled growth and characterization of the optical properties, *CrystEngComm*, 2017, **19**(37), 5591–5603.

18 E. Mendoza-Mendoza, A. G. Nuñez-Briones, L. A. García-Cerda, R. D. Peralta-Rodríguez and A. J. Montes-Luna, One-step synthesis of ZnO and Ag/ZnO heterostructures and their photocatalytic activity, *Ceram. Int.*, 2018, **44**(6), 6176–6180.

19 V. K. H. Bui, D. Park, T. N. Pham, Y. An, J. S. Choi, H. U. Lee, O. H. Kwon, J. Y. Moon, K. T. Kim and Y. C. Lee, Synthesis of MgAC-Fe_3O_4/TiO_2 hybrid nanocomposites via sol-gel chemistry for water treatment by photo-Fenton and photocatalytic reactions, *Sci. Rep.*, 2019, **9**(1), 11855.

20 T. N. Nguyen, V. V. Tran, V. K. H. Bui, M. Kim, D. Park, J. Hur, I. T. Kim, H. U. Lee, S. Ko and Y. C. Lee, A Novel Photocatalyst Composite of Magnesium Aminoclay and $TiO_{(2)}$ Immobilized into Activated Carbon Fiber (ACF) Matrix for Pollutant Removal, *J. Nanosci. Nanotechnol.*, 2020, **20**(11), 6844–6849.

21 S. A. A. Vandarkuzhali, M. P. Pachamuthu, V. V. Srinivasan, S. K. Mohamed, H. S. M. Abd-Rabboh, M. S. Hamdy and V. T. Balamurugan, Efficient reduction of dyes to leuco form over silver nanoparticles on functionalised SBA-15 and aminoclay, *Int. J. Environ. Anal. Chem.*, 2020, **1**, 1–14.

22 V. K. H. Bui, D. Park, V. V. Tran, G.-W. Lee, S. Y. Oh, Y. S. Huh and Y.-C. Lee, One-Pot Synthesis of Magnesium Aminoclay-Titanium Dioxide Nanocomposites for Improved Photocatalytic Performance, *J. Nanosci. Nanotechnol.*, 2018, **18**(9), 6070–6074.

23 V. K. H. Bui, T. N. Pham and Y.-C. Lee, One-Pot Synthesis of Magnesium Aminoclay–Iron Oxide Nanocomposites for Improved Photo-Fenton Catalytic Performance, *J. Nanosci. Nanotechnol.*, 2019, **19**(2), 1069–1073.

24 Y. Pei, C. Xiao, T.-W. Goh, Q. Zhang, S. Goes, W. Sun and W. Huang, Tuning surface properties of amino-functionalized silica for metal nanoparticle loading: the vital role of an annealing process, *Surf. Sci.*, 2016, **648**, 299–306.

25 T. C. Perrotti, N. S. Freitas, M. Alzamora, D. R. Sánchez and N. M. F. Carvalho, Green iron nanoparticles supported on amino-functionalized silica for removal of the dye methyl orange, *J. Environ. Chem. Eng.*, 2019, **7**(4), 103237.

26 R. S. Zeferino, M. B. Flores and U. Pal, Photoluminescence and Raman Scattering in Ag-doped ZnO Nanoparticles, *J. Appl. Phys.*, 2011, **109**(1), 014308.

27 W. J. Li, C. Y. Kong, H. B. Ruan, G. P. Qin, G. J. Huang, T. Y. Yang, W. W. Liang, Y. H. Zhao, X. D. Meng, P. Yu, Y. T. Cui and L. Fang, Electrical properties and Raman scattering investigation of Ag doped ZnO thin films, *Solid State Commun.*, 2012, **152**(2), 147–150.

28 S. Gayathri, O. S. N. Ghosh, S. Sathishkumar, P. Sudhakara, J. Jayaramudu, S. S. Ray and A. K. Viswanath, Investigation of physicochemical properties of Ag doped ZnO nanoparticles prepared by chemical route, *Appl. Sci. Lett.*, 2015, **1**(1), 8–13.

29 Y. Cai, H. Fan, M. Xu and Q. Li, Rapid photocatalytic activity and honeycomb Ag/ZnO heterostructures via solution combustion synthesis, *Colloids Surf., A*, 2013, **436**, 787–795.

30 F. J. Manjón, B. Marí, J. Serrano and A. H. Romero, Silent Raman modes in zinc oxide and related nitrides, *J. Appl. Phys.*, 2005, **97**(5), 053516.

31 T. N. Pham, S. T. Tanaji, J.-S. Choi, H. U. Lee, I. T. Kim and Y.-C. Lee, Preparation of Sn-aminoclay (SnAC)-templated Fe_3O_4 nanoparticles as an anode material for lithium-ion batteries, *RSC Adv.*, 2019, **9**(19), 10536–10545.

32 S. A. Ansari, M. M. Khan, M. O. Ansari, J. Lee and M. H. Cho, Biogenic Synthesis, Photocatalytic, and Photoelectrochemical Performance of Ag–ZnO Nanocomposite, *J. Phys. Chem. C*, 2013, **117**(51), 27023–27030.